Fabrication and Characterization of 2-D Materials based Solar Cells

By

Asad Javaid

School of Chemical and Materials Engineering
National University of Sciences and Technology
03,2020

Fabrication and Characterization of 2-D Materials based Solar Cells

Name: Asad Javaid
Reg.No: 00000203830

This thesis is submitted as a partial fulfillment of the requirements for the degree of

MS in (Materials And surface Engineering)

Supervisor Name: Dr. Aftab Akram

School of Chemical and Materials Engineering
National University of Sciences and Technology
H-12 Islamabad, Pakistan
March, 2020

Dedication

I dedicated this project to my Parents and Teachers

Acknowledgements

I would like to express my genuine gratitude to my Supervisor **Dr. Aftab Akram** for his support, encouragement and technical guidance in my Research project that has made this thesis possible.

I would like to acknowledge my GEC **Prof**. **Dr. Zakir Hussain** and **Dr. Iftikhar Hussain Gul** for support and guidence.

I would also like to acknowledge **Prof**. **Dr. Arshad Saleem Bhatti And Dr.Shumaila Karamat** from COMSATS Islamabad for their guidance and support.

Last but not the least , I would like to thank my Family for their support especially my Parents who have prayed for my success in life and the hereafter.

Asad Javaid

Abstract

A simple and cost effective technique is used to Fabricate 2-D Material based solar cells. In this work MoS_2 and Graphene is fabricated by Exfoliation Method and by Chemical Vapour Deposition (CVD). By using CVD, growth of MoS_2 Nano-wires form on Silicon substrates while by Exfoliation of graphite powder in DMF solvent is done to form Graphene and exfoliation of Bulk MoS2 powder is done in DMF to form mono or Bilayer MoS2. These Materials were characterized by Raman Spectroscopy , X-Ray Diffraction (XRD), UV visible spectroscopy, Atomic Force Microscopy (AFM) and Scanning electron Microscopy (SEM). Solar cell device is successfully fabricated on doped silicon substrate and tested by I-V curve of Solar Simulator. Silver back and front metal contacts were deposited by Sputtering method. 4.02% highest efficiency were obtained.

Table of Contents

List of Figures

Chapter 1

Introduction

We all know that earth is having no replacement so it is for everyone. Fast property of being diminished is on one side and the significant harmful effect of industrial development is on planet is another side. Scientific illusion of global warming have been changed recently to the field of real life [2]. Only renewable energy is an answer to the need of paradox of this coupling with ever growing energy [3]. Some of the alternate technologies include geothermal ,wind ,biomass and solar energy. Sun is consider as a greatest renewable source of light and energy , so the solar energy are the ability to fulfil long time energy demands of mankind, out of the mix. Which can be categorized as passive as well as active technologies. In case of passive technologies, designing an energy efficient building making use of maximum occurrence light is an analogy [4]. Whereas, in case of active solar technologies Solar cells offering the most authentic product of transferring of light energy into power energy .

As abundant, cost associated with this technology is the limiting factor. This issue of limiting factor can be resolved if we use equality with the fossil fuel to drive energy plants in future technologies to succeed. Moreover, stability and efficiency of technology is enhanced. Thus, solar cells playing vital role in power generation. This technique meet the energy requirement in the universe[1].

1.1Generation of Solar Cells

While the invention of photovoltaic (PV) result, we are divide such PV devices in three generations which is based mostly on timelines of their beginning. Out of which, the 1st generation of the PV device consists of solar cells like the single junction that is handled pure silicon biscuits created to join the demand for functions of satellite. Efficiency is achieved by 25% and η is inadequate to about 30%. [6]. While enhancing the material as well as processing cost of generating such PV technologies led to its second generation. The greatest effective technologies in this group were copper indium gallium (di)selenide (CIGS), Cadmium telluride (CdTe) and amorphous Si. For lab scale devices, this class materials has highest recorded efficiency at 19% and for commercial module it is 14%. In minimizing limiting factor of first generation, for second generation failure in the attaining big area of thin films as well as lower efficiencies has been the limiting factor after effective in focusing the high quality material and cost related with first generation technology. In the period of less cost tools, advent of the organic PV devices as well as and Dye-Sensitized Solar Cell (DSSCs) are newer materials and concepts. Demonstrating the applications on flexible substrates presenting building integrated design and unique opportunities indicated a new model in renewable energy environment[7]. For over a decade, that generation of solar cell technology has been in broad research and has attained a maximum efficiency of 12% for DSSCs.

1.2. Cost

To meet our energy needs, it is sufficient to use 0.2% incident solar radiation. The cost-limiting factor associated with these technologies. Coal at .0 0.04 / kWh (kWh), while the cheapest power source is a power plant, it costs 20 0.20 to 35 0.35 for similar power from PV. Processes related to the production of PV modules include semiconductor absorbers, PV cells, construction of PV components and installation of modules. In the final stage, the cost of power storage devices is also included.The total cost, 30-50% of the cost of the system's PV modules is associated with the high cost associated with off-grid systems associated with storage equipment [8]. At $ 1 / W for the entire PV system, the PV module actually costs $ 0.5 / W. reported, C module costs $ 0.65 / W, which is approx. Thin film technologies require deep power, concentrated processing and very thin layers of semiconductor are less expensive than Si modules. The 17.5% module cost efficiency is 0.61 / W, which is expected to decrease around $ 0.35 / W in 2018 in the case of CDT modules. For module like CIGS with η =15.7%, the segment total is valued at 0.64 / W dollar 6. Being an adult technology, there is no doubt that crystalline technology will dominate the PV market. C-C's current market share is approximate at 90%, with technologies related to thin film contributing 13%. Significant cost reductions have occurred over the years, but material shortages and processing costs have hampered the fulfilment of the potential of related technologies.

We need energy intensive techniques in C-C processing to achieve metallurgical grade C as a solar grade material. CIGS and CdTe involve elevated temperatures and processing of elevated vacuum at 450–650 ^{o}C. Epitaxial uptake by modules of gallitum arsenide (GaAs) is required, so providing them is very expensive. By the year 2050, the capacity of 5TW PV modules will be required to generate 16% of global electricity demand. Under current methods, C-C is more expensive. It is imperative to develop low-cost processing and technology based on land-rich materials to meet the estimated costs. Abundant and reliable materials Low cost supply, toxicity is low and high stability are main requirements for PV cell production at very low cost. These properties differ from each other and it is a challenge to find a material that is suitable for the material material society [9].

The introduction of 2-D material-based solar cells is a recent breakthrough in PV methods, recording an efficiency of 11.1%. In addition, it uses compatibility with earth-rich materials, lower in temperature key processing, high annihilation coefficients and wide absorption spectrum, bipolar transport charge and longer in diffusion length, flexible surface, that category of material regenerative energy landscapes. Stands to replace [10]. Poisonousness and long stability stay a challenge, but it remains the truly attractive applicant for the upcoming of good absorbent class PV devices.

The material belonging to the pericytes is composed of the crystalline assembly of calcium titanite, that is ABX3. Many other materials that adopt these structures have sensational applications such as insulating, thermoelectric, piezoelectric, semiconducting, conductive, anti-ferromagnetic and superconducting known by virtue. We must synthesize these perocytes by solid state mixtures of basic compounds at little high temperatures around > 1300K range. We can also achieve this goal of synthesizing by the solution drying of the antecedent salts and finding vital appliances in print-able electronics due to the solutions that provide semiconductor properties. In describing the composition of perovskite class materials as ABX3, A,B and X is an ion with dimensions is different, but A is larger than X. We illustrate the assembly of the material in Fig. 1.2. The facts of the element of tolerance T and the octahedral factor μ13 determine the potential structure and crystalline solidity, where

T is well-defined is the ratio of bond length A to X in X in a solid model X, which are octahedral. The narrow variety of T values determines the 0.89–1.0 cubic structure, whereas the lesser values of Temperature alleviate the lower isometric structures.

Due to its low stability, it is oxidized to SnI_4, but has relatively high safety in Pb. Therefore the basic mixture is methylamonium lead triode (CH_3 NH_3 PbI_3).

1.3. Perovskite-Sensitized Solar Cells

DSSCs are precursors of perocyte solar cells. When we talk about specific DSSCs, mesoporous N-type titanium is sensitive to light-gripping dye in a active redox electrolyte. For efficient absorption of photons, the maximum internal surface area generated by porous titanium is necessary for entire absorption in the absorption range of 10 µm dye. When we talk about solid state DSSCs, it is impossible to talk about a 10µm thick active layer, there are many factors that make the active layer thickness less than 2µm. Alternatively, the quantum droplets and thin film semiconductors in the active layers, in very thin layers, have full light absorption, while the photosensitivity must be pushed into the near infrared (NIR) at 25,26, 27, 28,29. Background, for more efficient photosensitizers for DSSCs, via the first Perov stike-Sensitized Solar Cell. This was reported between 2006 and 2008 between Miyasaka and colleagues. CH_3 P_3 PBI_3 and CH_3 NH_3 PBr_3 absorbers were employed with a poly-pyramidal carbon black composite solid-state hole conductor or an iodide triode redox pair [12]. The difference in efficiency of full solar energy conversion is between 0.4% and 2%, which has been successfully measured for solid-state and liquid electrolyte cells, respectively.

The Peer-Review Report for Perocyte-Sensitive Solar Cells was first published in 2009, with an absorbable CH_3 NH_3 PbI_3 3.5% efficiency in iodide / triiodide redox doubles. In Fig. 1.3, the plan sensitivity of the materials likrmaterlic halide(Organic) for the solar cell , by magnifying the surface morphology NG Park and colleagues achieved 6.5% efficiency while maintaining liquid electrolyte. Peroxide is the basis for the dissolution and decomposition of percovite into liquid electrolyte to overthrow blocks in a sensitive solar cell. As a result the stability of solar cells is low and deteriorates in minutes. Miyasaka and colleagues alleviated the problem in 2008 when they replaced the electrolyte with a solid state hole transport medium.

In many inorganic organic solvents methylmoniumtrihalogen is thought to be relatively insoluble, which is thought to be possible first by percutaneous sensitivity and then by infection to organic pore conductors. For this reason t. Murakami and T. Miyasaka and. MR Tezel and colleagues (2,2 (7,7) -tetracis- (n, n-dipmethoxyphenylamine) 9,9 (-probrophyllofluorine) (spiro) developed in collaboration with solid-state perocyte to develop solar cells in the park) -Omet CH3NH3PbI3 Cl xClx composite halide perocyte and CH3NH3PbI3, 12 complete transporter 34 with 8 and 10% maximum full solar energy conversion capacity are used as holes.35,36, respectively.

This success was noted in the Solid State DSSC performance along a record capacity of over 780. It’s possible due to higher exposure risks in the form of strong absorption over a wide range of conventional colors, resulting in a complete absorption of at least 500 nm in film thickness. This is particularly advantageous for solid state particles, where light absorption and photo cross production are generally limited by the need for a film thickness of 2 μm[11].

1.4. MesoporousTiO$_2$ Scaffold

The most efficient stable pericyte cell was first manufactured by spin coating in 2012, but is a butyrolactone key containing PbI2 and CH3NH3I equalizers. This led to the semi-annual nanoparticle description of CH3NH3PbI3 on TiO2 [13]. While the exterior is not completely covered with nanoparticles, it is clear that photo-activated electrons have been transferred from CH3NH3PbI3 to TiO2. The cell with 0.6 μm titanium film achieved 9.7% PCE and a wok of 888 mV. A filler component of 0.62 indicates poor aperture filling with the spirometer and consequent poor boundary between the (HTM), the active membrane and the (ETM) [7].

The device structure confirmed the pore carrying properties of Cell. It attained 5.5% PCE by FTO / 100 nm thick TiO2 with hole resistance and electron transport equipment. A 100 nm increase from TiO2 improved PCE by 8% 39. MotPlayshotkie was used to determine the decay area among TiO$_2$ and Compound, this composition is mentioned to as the hetero junction percovasite SS. The shunt resistance(large) 540 factor affected weak filler-factor (FF) and the low external quantum capacity (EQE) in the long wavelength range of 800 nm.

Ambi-polar properties of cmpound have been informed by Hio et al., Built on (TFT) assessment, with a marginally tougher P-type sort. Still and transient photolumination (PL) corrosion studies have shown that the charge transporters replace the CH3NH3PbI3 / poly (triarylamine) HTM interface with some charge separation in TiO2. The Superior PCE in the Spiro-Metad system is attributed to the thinner (M30 nm) HTM layer related to the Spiro-Metad HTM (N500 Nm), resulting in lower series resistance. Devices that do not have HTM have demonstrated poor performance of CH3NH3PbI3 systems that require physical chemistry study.

Percovite light harvesters with one dimensional nanostructures have also been reported. Rutile TiO2 (long0.6 longm length) achieved 9.4% 41 PCE with photoactive CH3NH3PbI3. Growing the length from the 0.6 to 1.6 m reduced the photovoltaic operation. By the increase in length of nano rods the bent nano rods had problems filling the holes with spores-meadow. A change in the structure accumulated from the nano dot to the active layer can beat this problem. Br Br I Mixed Pervocyte CH3NH3PbI2Br with Tivo 2 achieved 4.87% PCE, slightly higher than CH3NH3PbI2B for CH3NH3PbI2Br mixed halide perovocyte 42 high wok.

While bearing in mind electron injection in the mesoporous titania from the photoactive layer, the voke is concluded by the change in fermi level of the TOO2 and the homo amount of HTM. Despite such a large change in wok, the homo levels in PCBTCP and P3HT (PCBTDPP: 5.4V and P3HT: 5.2V) are not only 0.02, but also cause mild filtration and chemical interaction levels [14]. The PCBTDP-based device produces high volume as a result of increased light filtration and strong chemical interaction effects, resulting in charge re omb synthesis and shift up the organization level. These findings indicate that the reasons other than power readings should be considered for the HTM selection.

1.5. Meso-Superstructured PSCs Based on Non electron Injecting Oxides

In the photovoltaic cell, the composite percovasite alumina layer results in CH3 NH3 Pb12 Cl 10.9% mixed PCCOS. Due to the different band edges of the alumina and perocyte active layer, this structure of device is known as a "mesospastricated solar cell" where electrons arephotogenerated are not moved so that they move through the scaffold to carry the photoactive layer. The spin coating is more stable in air than other compound. In the perovastic structure, the small size of the Cl of - stabilizes the ions. The O_3-CH_3 NH_3 Pb_12 Cl system in Al_2 produced more wok ఽ$^{\delta}$ than the TiO_2-CH_3 NH_3 Pb_12 Cl. The study of photoinduced spectroscopy concluded that the difference was due to the differential behaviour of the photogenerated electrons in the two systems [15, 16]. The differences due to the photo-induced spectroscopy study were due to scaffold layers that could be processed at lower temperatures when the high-temperature annealing phase was excluded because the electrons produced were not injected or transported into the mesoporous membrane. 12.3% PCE value 47, achieved by low-temperature processed mesosphere structure solar cell (150 ° C dried all 2 o 3 mesoporous layers). When the width of Al_2 O_3 changes, the skeleton layer from 0 (no scaffolding) ca. Excessive CH_3 NH_3 formed at I_3-xCl_x over 400nm, 80nm dense alumina film, but no limiting layer formed at 400nm Al_2 O3 film thickness. From the 80nm Al_2 O_3 layer, the highest PCE is observed, resulting in the highest JSC, with the 400nm layer eventually showing an improvement in the FF of the VOC and Al_2 O_3. Therefore, we can say that the increased systolicity in the active layer of the perocyte increases the JSC, although the VOC and FF pins are due to orifice-free perovascularity. To achieve a PCE of 7.16%, nanoparticle suspensions of alumina (5 wt% Al_2 O_3) and co-deposited percovite precursors in DMF are used.

CH_3 NH_3-PbBR_3 CH_3 NH_3 With a larger bandwidth of 2.3eV compared to PbI_3, it is used as a light transporter and an electron transporter using the concept of mesonoporstructure.

The V_{OC} of 1.30 V49 were obtained with the tool assembly of Al2O3 / CH3NH3PbBr3 /, k - dialkylperyle- nediimide (PDI). The huge vacuum can be clarified by the injection of photo3 excited electrons into the L3O (4.2 eV) of CH3NH3PbBr3 of PDI and alumina scaffolding. The mesoperstructural concept was also assessed with the Z3O2 mesoporous scaffolding with the compound light harvester material, which exhibits considerable photovoltaic movement, Voc of V900 mV, which is less than tit5050. Resistance spectroscopic studies use three electrode electrochemical cells, confirming that zir-conia is not scaffolding. In compare to the mesoporous membrane, it shows that photogenerated of electrons were not be inserted into the zirconia scaffold 50. This relative study concluded that $CH_3NH_3PbI_3$ can accrue charges due to high density states (DOS). 10.3% higher efficiency was described for CH3NH3PbI3,43, the sensitivity of ZrO2 scaffolding with VOC 1.07 V.

1.6. Planar Heterojunction Structured Cells

Thermally co-evaporating CH_3NH_3I and $PbCl_2$, depositing $CH_3NH_3PbI_3$ F xCl_3 with a thin layer of TiO_2 on the FTO caused in PCE 15.4% to 51. This demonstrates the bio-functional estate of perovskites, i.e. photo-excitation and the transport of charge. Therefore a mesoporous oxide layer is not mandatory. The vapor deposited perovskite coating demonstrated better PCE on the treated PCE on the solution due to better morphological self-control and the creation of a identical flat. Although it is easy to find a flat $CH_3NH_3PbI_3$ x xClx active layer through solution handling, it is hard to create a regular active-layer of $CH_3NH_3PbI_3$ by using solution.

The P3HT / PCBM alloy are widely revealed in organic photovoltaic(cells) applications. P3HT were converted to a photoactive layer with CH3NH3PbI3, which achieved 3.9% PCE in planar heterojunction solar cells. 52 Obtained with improved pedability: activated with percocyte coated-butyrolactone solution [16, 17] with PMS coated ITO substrate with DMS solution compared with membrane. . A device structure based on TiO2 / CH3NH3PbI3 x xClx / P3HT, when ITO substrates were handled alog C_{60} self-built monolayer, they achieved superior photovoltaic performance. PCE upgraded from 3.82 to 6.78% , with addition of self-constructed monolayers. This was completed with major increases in both the Jsc and Voc53. The idea of a hybrid planar heterojunction cell joining a 285 nm better thick layer of CH3NH3PbI3 was recently inspected. Sandwich made the layer(Active) between the poly conveying (polytpd) coating (10 nm thick) and the PCBM coating (10 nm thick) 54%. The accumulating layers were treated with a chlorobenzene spin coating, although the layer that is active was deposited by the heating agents CH3NH3I to 70 ° C and PbI2 to 250 C.

1.7. Flexible Perovskite Solar Cells

It is possible to make flexible surfaces from low temperature solutions of perocyte solar cells. Such architectural assets have considerable potential to incorporate this technology into a wide variety of applications. CH3NH3PbI3 N: PSO and PCBM as the active layer with XClx PEDOT receive 6.4% of the ITO coated PET surface PCE on an inverted device structure, which have been inspected as electron discriminatory contact and the hole transport, respectively. 55. 10.2% higher PCE achieved. Constructed using low temperature solution processing methods using the device structure of ITO[18]. The PEN surface coated with ITO also plays an important role. The performance of the wearable percocyte-based power source achieves a PCE of the 12.2%, only with 5% damage on 1000 bending wheels of 10 mm in radius [109].

1.8. Hybrid Multijunction Solar Cells

At current capacity, perovite solar cells can be used extensively in tandem cell outline, with machineries such as existing crystalline silicon and TT solar cells CZTSSe, CIGS59 and CIS. The top perovskite cell is 20 mA cm and the silicon cell producing VOK2 and 1.1V, 0.75V VOC is expected to achieve an FF of 0.8 and 29.6% 61 efficiency. This is made possible by existing technologies that optimize bandwidth expansion and strengthen tandem cell architecture [19].

1.9. Fourth generation Solar cell:

The latest technology introduced in solar cell is fourth generation solar cells. These cells composed of 2-D materials based. This 4th generation solar cell are mostly based on Graphene and M Molybdenum disulfide (MoS2). While these 2-D materials are reflects very good photovoltaic properties and behaves as a active layer n solar cell structure[2].

1.10. Material:

Graphene is 2-D materials , known as allotropic kind of carbon, in which atoms are arranged in shape of 2-D lattice like honeycomb. Isolation methodology is the cause of its success . The created technique allow to separate the 2-D material on the high of a 300-nm-thick silicon oxide wafer. The van der Waals interaction is weak incorporated grip between graphene and also the wafer, and on top side of the Silicon wafer, it makes a 2D material possible for the movement , moving it from the one substrate to a different or maybe having it suspended over a channel, maintained from one side Stand within the production methodology, graphite shows a vital part meanwhile three-dimensional 3D material is itself fabricated from graphene planes fixed attached by the van-der-Waals forces. The cleverness of the strategy was then to find some other ways of peeling one layer of graphene from graphite. The Monolayer of graphene attracts $\pi\alpha \approx$ 2.3% of white light transmittance (97.7 %), where α is the constant of fine- structure High Young's modulus is around(~1,100 Gpa) High fracture strength is around (125 Gpa)[21] . Each is characterized by a proportional decrease in optical transparency and sheet resistance with increasing graphical layers such as optical transparency, sheet resistance relationship and hence layer mass. The layer of graphene shows an optical transparency of 97.7%. Around 90.8% optical transparency is present in a 3-layered graphene stack and therefore by adding every layer corresponds to a two.3% reduction in the optical transparency. one graphene sheet exhibits a resistance of two.1 kΩsq-1 and 350 Ωsq-1, it is single layer of carbon atom and it has a unique properties in Photo voltaic applications[22].

At This Time, some great efforts on the third generation solar cells are being made in the laboratory, and developed by new companies/Industries and for the most part is not commercially available.

MoS2 is 2-D material of single-layer atoms and multi-layer had been achieved during the first periods of the 20th century. In recent years a great attraction found in transition metal dichalcogenides (TMDCs) like (MoS2 , WS2) due to their rare and interesting optical, physical, and photovoltaic properties, which differentiate them from their parent bulks. Semiconducting MoS2 is considered as one of the most important 2D materials which overcomes the short coming of zero band gap of graphene and extends its applications in modern electronic and optoelectronic devices. MoS2 has a bandgap of layer-dependent with a direct to indirect bandgap which varies since 1.8 eV in the monolayer to the 1.2 eV in parent bulky structure[23]. The unique optical properties of MoS2 and strong light-matter interaction offer the opportunities in exploring next-generation microelectronics and photovoltaic devices (Solar cell, Transistors)[22].

Chapter 2

Experimentation

2.1.1Thin film deposition

The thin films are supported over glass or polymeric substrates to gain efficient properties and phenomenon by them. Substrates involve properties of the thin films[3]. The deposition of the thin films will be done by applying various techniques in which vacuum is used. The techniques are:

1. Atomic layer Deposition (ALD)
2. Pulsed laser Deposition (PLD)
3. Molecular Beam Epitaxy (MBE)
4. Chemical vapor deposition (CVD)
5. Physical sputtering (DC/RF)
6. Spray Pyrolysis
7. Sol-gel method

2.1.2Atomic Layer Deposition (ALD)

ALD is controlled growth process. In this process, the precursors are introduced by purging processes. The gases will react and grow on the substrate's top surface. The growth processes which happen in ALD are such as:

1) Introduction of gasses in to the growth chamber.
2) Inert gas is purged to remove any precursor which has not taken part in reaction
3) Second precursor is introduced in to the growth chamber for reaction.
4) Cleaning the chamber with the inert gas again.

Reactive precursors react on the substrates for reactions. The reactions occur at ambient temperature and pressure conditions. The growth of the films can be done even at low temperature conditions. ZnO deposited films grown by the ALD process have been utilized in photovoltaic devices (solar cells), as the transparent conducting oxide coatingin inorganic and the organic PV devices, and as the n-type associates of the p-type materials present in the solar cells[4].

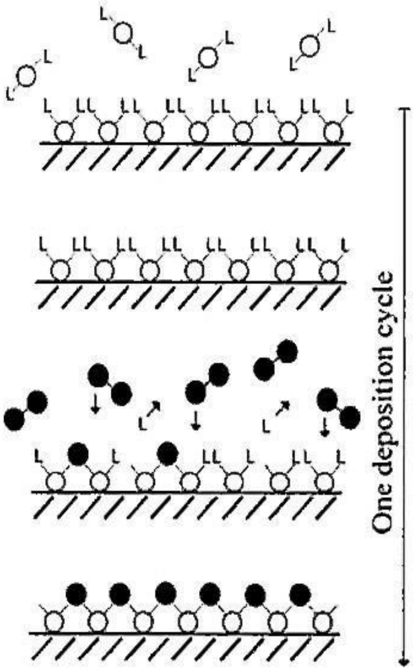

Figure:1. Schematic illustration of ALD cycle

2.1.3 Pulsed Laser Deposition (PLD)

It is a wafer-thin film deposition technique in which pulse laser is utilized to make molecules which are then deposited on the substrates. The raw material to be deposited is evacuated inside the chamber. The material is evaporated from the target of the material and after that vaporization takes place and the material is depositedlike a thin film on the substrate[5].

2.1.4 Advantages:

- Facile technique for the deposition of the thin films of materials.
- The stoichiometry of target is maintained in deposited films.

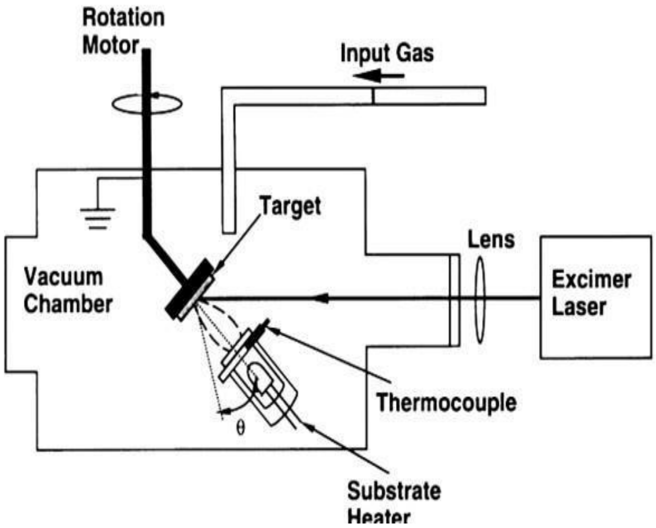

Figure:2.Schematic of a PLD system

2.1.5 Molecular-beam Epitaxy (MBE)

This process involves generation of material's precursors. The reactions occur at ambient temperature and pressure. Vacuum is introduced to upsurge the mean free path for transport of gas molecules. The fluxes of gas intake can be changed and shutter can be used to cover samples in area in which we do not want to have deposition[6]. Schematic of MBE is shown in the Figure 3.3:

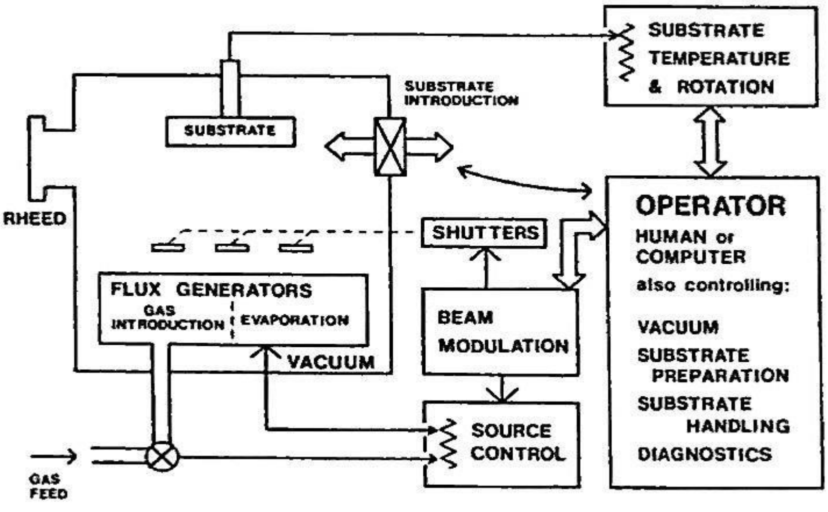

Figure:3. Schematic representation of MBE process

The electron-cyclotron-resonance is used to generate the oxygen plasma . The reactions can be carried out at low temperatures via varying pressure conditions.

2.1.6 Chemical Vapor Deposition (CVD)

It is the process in which volatile reactant gases are introduced in the reaction camber which then react chemically on the desired substrate surface to form films of materials that are to be introduced[7].

Precursors. Thin films of the materials $_{(s)}$ + By-products $_{(g)}$

Typically simple sputtering of the target material has disadvantages such that:

- Structural imperfection and defects
- Non-uniform distribution of dopant elements like (Al, Ga, In, etc.)
- The variability of the electrical properties in the deposited film.

So, In demand to beat such harmful effects, CVD has been commonly used for the preparation of pure/doped ZnO and thin films of other semiconductor material for solar light harvesting[8].

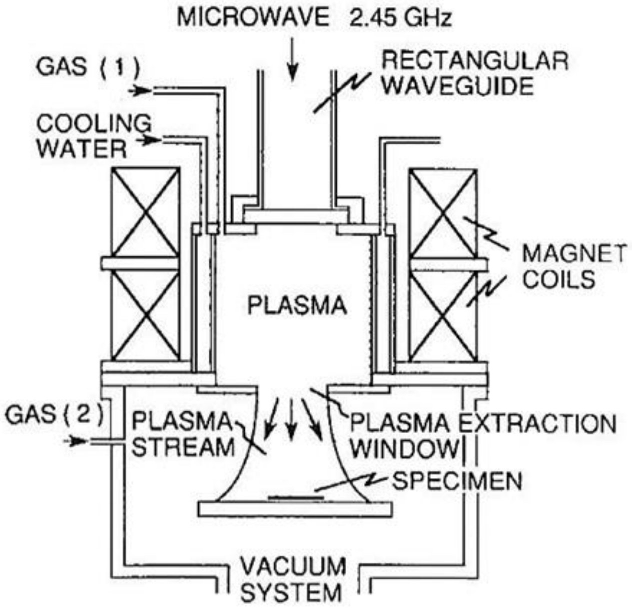

Figure:4. ECR plasma enhanced CVD Reactor

2.1.7 Physical vapor deposition:

It non-thermal evaporation process. The particles are sputtered with much high energy to provide higher mean free velocities for gasses. In typical a sputtering process plasma is generated in the gas chamber in which the reaction is taking place. Usually the plasma is introduced by purging Ar gas molecules with high energy which knocks off electron from the target materials[9]. These knocked off molecules then go to substrate surface to deposit the thin films.

The physical vapour deposition can be done by DC or RF sputtering as shown schematically in Figure 3.5. in DC sputtering, the plasma is directly use to knock off molecules from the target material. However, if magnets were used in combination with the sputtering system, then it's known as magnetron sputtering[10]. RF magnetron sputtering is usually done for non-metallic materials.

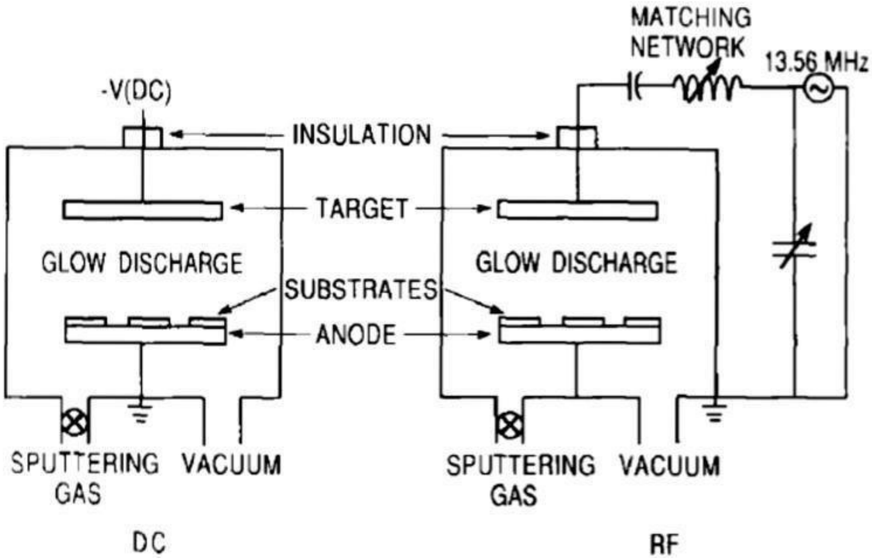

Figure:5. Schematic of sputtering systems: (a) DC, (b) RF

2.1.8 Spray Pyrolysis

This technique is used to deposit the thin films of metals or metal oxide nanoparticles on the substrate. It involves liquid spray of molecules or materials to be deposited on the heated substrate[11]. This technique is most common as it is used for the preparation of thin films because of its modesty; vacuum system is not required and therefore cheaper method for the large area coverings[12].

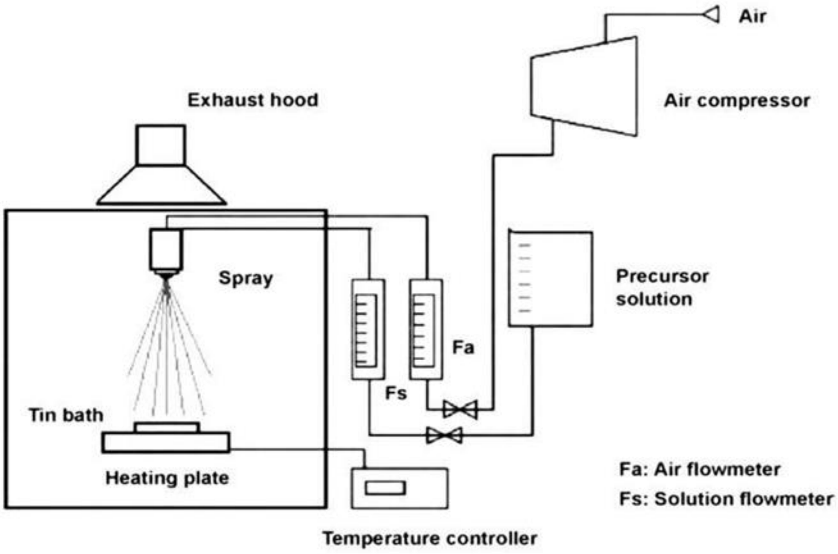

Figure:6. Schematic representation of spray pyrolysis process

2.1.9Mechanical exfoliation:

In this method, the layers are separated by applying some mechanical forces[13]. Graphene was synthesized by this method using bulk graphite by **“scotch tape method”[14]**. In this method, high-quality mono sheets can also be formed. This method is popular as it produces intrinsic sheets and a large area of research is focused on it now.

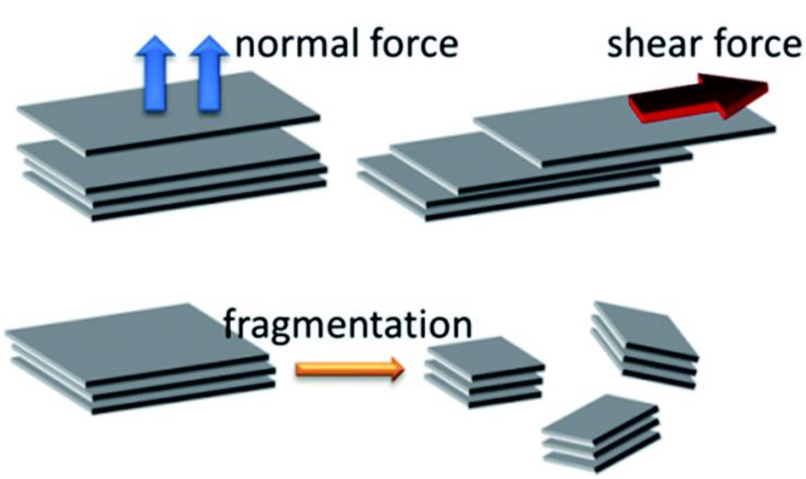

Figure:7. Mechanical Exfoliation of 2D materials

2.2.0Merits:

- Generally, by this method, pristine quality sheets are obtained.

2.2.1 Demerits:

- Low yield is obtained in this process.
- Also in this method, there is lack of scalability76.
- The method is not applicable for production on a large area scale.
- Sheet size and thickness controlling is an issue.

2.2.2 Liquidphase exfoliation:

In this method, solvents are used to intercalate the layers of compound. Those solvents were used whose surface energy match up with that of the crystal lattice of the layered material[15]. Sonication produces single and the multilayer nanosheets are become stable in the presence of a suitable solvent/surfactant present in reaction mixture or dispersion[16]. Some surfactants may also be added in them to obtain well-defined structures. Sonication assisted exfoliation is now used extensively for preparation of mono-, few-layered structures from bulk. In sonication sound energy is applied which results in shear forces. Cavitation bubbles are produced which when collapse peel off the layers[17].

Selection of solvent is crucial choice, i.e., it must expedite the delimitation process. It should sustain highly stabilized dispersions with a high concentration of 2D exfoliated sheets. Sometimes a combination of solvents may also be applied for efficient exfoliation of materials. In solvents, N-methyl-2-pyrrolidone (NMP) is a widely used . NMP has a surface energy of ~40mJm-2 which matches with the surface energy of the multi-layered materials[15]. In NMP, one can achieve stable dispersions of graphite with up to 40mg/ml has surface energy ~75mJm-2.

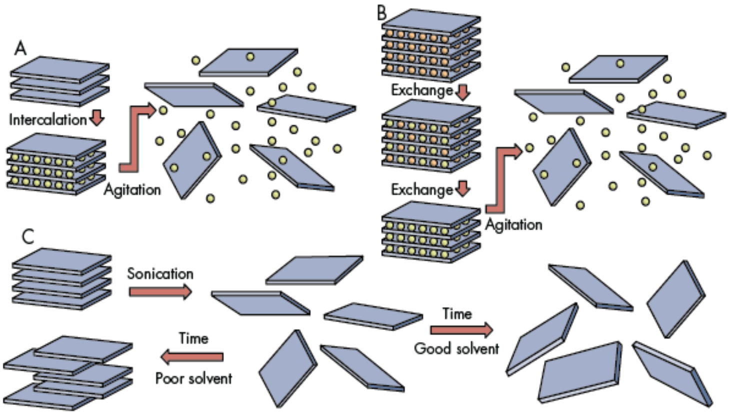

Figure:8. Liquid phase exfoliation of 2D materials

2.2.3Merits:

- High yield is obtained in this process.
- This method is the non-air sensitive.
- It does not include chemical reactions.
- The highly crystalline product is obtained.
- This method is so simple and cost-effective.
- Sheets of good scalability are obtained.

2.2.4 Demerits:

- The solution-based exfoliation contains residual chemicals present in them which can affect the properties of nanosheets like graphene. The solvent may be volatile and toxic too.

- This method can cause defects in 2D structures and reduce flake size to a hundred nanometers.

2.2.5 Bottom-up approaches:

Also, there are many ways to develop 2D materials via bottom-up approacheslike:

1. Wet chemical synthesis
2. Chemical vapor deposition

2.2.6 Wet chemical synthesis:

By this technique, the target materials are prepared using precursors, and chemical reactions take place in the solution. Certain surfactants are added to self-control the size, shape, and the morphology of target materials to be produced[18]. One extensivelyapplied wet-chemical methods for the nanomaterials include template synthesis, hydro or solvothermal synthesis, self-assembly of the nanocrystals, and the soft colloidal production[19].

2.2.7 Merits:

- All 2D materials sheets, metals, transition metal-oxides and the metal chalcogenides can be synthesized by this method.
- High yield of 2D nanomaterials at very low cost can be achieved.
- Control on morphology of nanomaterials is more in wet chemical methods.

2.2.8 Demerits:

- Hard to achieve single layer of 2D Nano sheets

2.2.9 Sol-gel Method

Sol-gel method is a wet chemical based method which is utilized for synthesis of metal oxides particles beginning from solution (sol). The precursor of the materials form an integrated joined network of molecules[20].

An extensive diversity of precursor materials is available. The precursors used for sol-gel synthesis are mostly metal alkoxides and metal chlorides. In this method, the precursors are dissolved in water which are then peptized to form precipitates of the materials[21]. Mostly metal oxides with uniform size distribution and good crystallinity are produced. These coatings are applied over the materials to have self-cleaning properties.

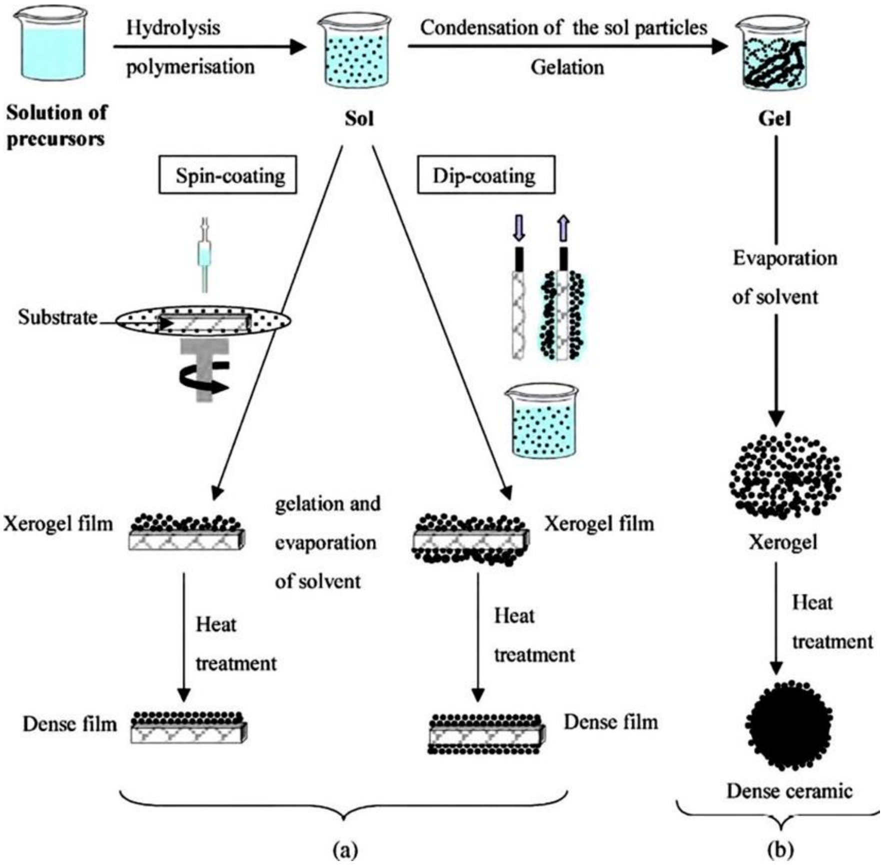

Figure:9. Systematic representation of all sol-gel processes

Now further we will discuss our experimental work. MoS2 and graphene prepared by wet chemical exfoliation method and by Chemical vapour deposition (CVD).

2.3.0 Exfoliation Method:

MoS2 and graphene were prepared by wet exfoliation method. The ratio of 20mg/mL graphene and MoS2 were dissolved in NMP and DMF both solvents. Initially in 80mL NMP 1.6g bulk powder MoS2 were dissolved and place in hard beaker. Place this beaker for sonication in probe sonicator for 48 hrs. this create a intercalated layer in solution. After sonication , centrifuge the solution for 45 min at 3000 rpm in 50mL plastic tube. The unexfoliated powder stick on walls of the centrifuge tube and exfoliated (thin) powder remain in solution as shown in fig.

This process is repeated same for Graphene exfoliation from graphite.

Probe sonicator

Prepare for centrifuge

After centrifuge unexfoliated materials stick on walls.

Exfoliated material are looks litt transparent as compared to unexfoliated

Figure:10. Exfoliation process of Graphite and MoS_2

2.3.1 Substrate preparation:

1. n-type c-Si wafers cleaning by RCA-1 and RCA-2 following by Hydrofluoric acid dip (2% HF diluted in deionized wafer DI) and rinsing in DI

2. Doping by using phosphorus oxychloride (POCl3) to form highly doped n+ regions

3. n+ was formed on both sides of n-type c-Si, therefore, single side etching to remove front side n+ region. Etching was done by potassium hydroxide (KOH). The concentration of KOH and the process temperature/duration were adjusted to etch the front side n+ and to create front side pyramids-like structures[22]. At this step the structure features: pyramids textures on n-type c-Si wafer/rear n+

4. Cleaning by RCA-2 to remove KOH-induced contamination followed by HF/HCl (10% diluted in DI) and rinsing.

2.3.2 Solar cell device Fabrication :

Solar cell structure were fabricated on silicon doped substrate has done by using spin coater.

Exfoliated MoS_2 were spin coat at 3000, 1000, 500 rpm for 30 second each and then dry at 75 ^{0}C for 20 minutes. Due to different rpm speed we got different thickness of layers and at 500 we got uniform layer on silicon substrate. After dry we again spin coat the graphene for same parameter and same rpm speed[23]. In the case of graphene we got uniform layer at 1000 rpm (checked by Optical microscope) and then dry at 75 ^{0}C for 20 minute. After deposition of materials we make silver (front and back) metal contacts by thermal evaporation method. In this method we grow 50nm thick back and 30 nmthick front metal contact[24].

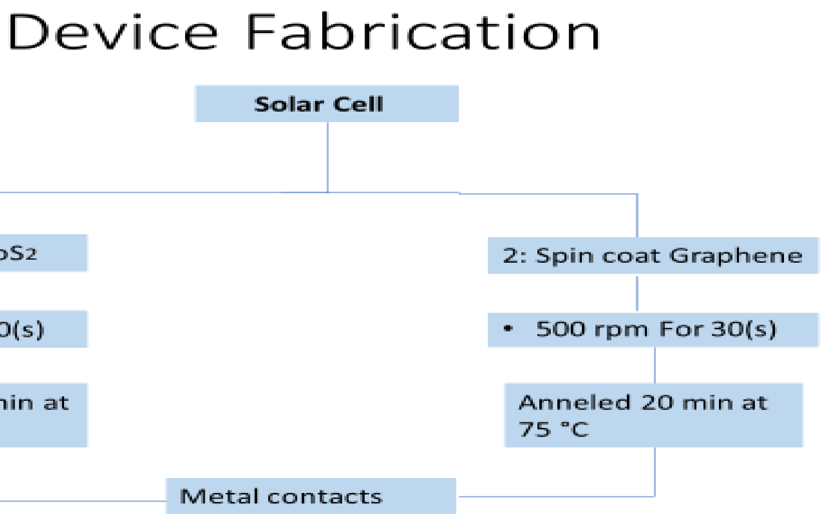

Figure:11. Schematic of Solar cell Device Fabrication

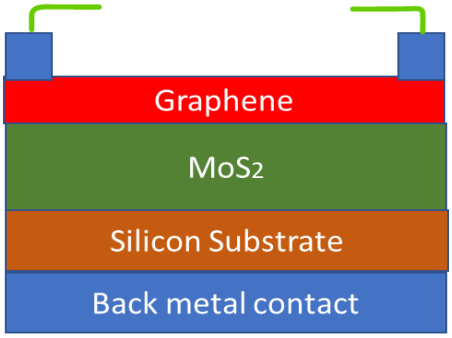

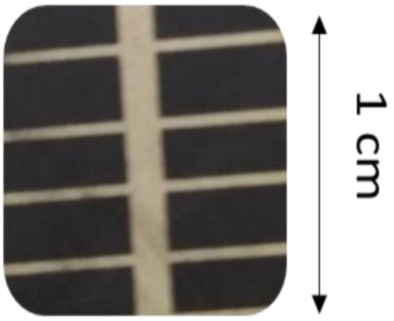

Figure:12. (a). Schematic of the graphene/MoS_2/n-Si solar cell. (b) An optical image of a Solar cell structuregraphene/MoS_2 thin film deposited onto a substrate. The scale bar is 1 cm^2.

2nd device preparation technique is by using CVD grown materials. We transfer Graphene and MoS2 on PMMA , shifted to silicon substrate and then make metal contact. The device structure is same as mentioned above.

Chapter 3

3.1. Charactrization Techniques

MoS_2 and graphene were characterized by the XRD, Raman Spectroscopy and Scanning electron microscopy (SEM) and solar cell were characterized by *IV*- Curves.

3.2. Scanning electron microscope (SEM):

In this method, fine beam of the electrons is focused over a specimen's surface. These electrons interact with the sample surface and photons or electrons are knocked off from material's surface in result. These knocked off electrons are then focused on the detector. The output from the detector modulates the brightness of cathode ray tube **(CRT)**.For every point where the electron beams are focused and interact, it is plotted on consequent point on CRT and material's image is produced[25].

The electron-surface interaction causes the release of **secondary electrons (SE), backscattered electrons (BSE)** and then **X-rays**[26]. Common SEM mode for detection is via **secondary electrons**. These electrons were emitted from near the sample surface. So, a pronounced and clear image of sample is obtained. It can reveal sample detail even less than 1nm in size. Also, elastic scattering of incident electrons also takes place and release **back scattered electrons**. They emerge from deeper locations as compared to secondary electrons. So, their resolution is comparatively low. **Characteristic x-rays** also emit from the atoms when an inner shell electrons knocks off from its shell[27].

We use SEM as it has easy sample preparation and we can figure our sample's morphology, chemistry, crystallography and orientation of planes. Magnification of SEM can be controlled from 10 to 500,000 times[28].

SEM analysis was completed using the scanning electron microscope (**JEOL-JSM- 6490LA**) with the operating voltage of 10-20 kV, spot size of 35-60, and running distance of 10mm. The images are recorded in SE mode at the both low and the high magnifications. **Fig 4.1 (a)** shows the JSM 6490LA SEM present in School of Chemical and Materials Engineering, National University of Science and Technology, Islamabad. **Fig 4.1 (b)**shows schematic of a typical SEM[29].

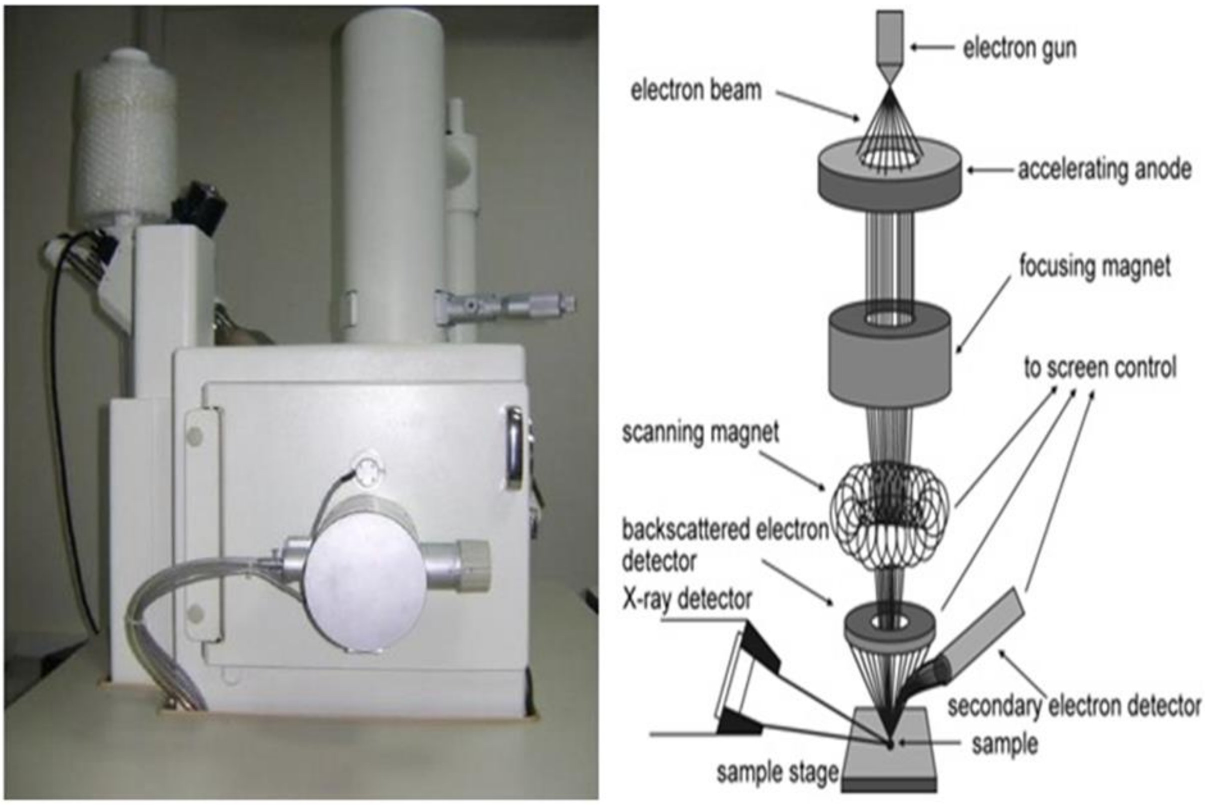

Figure:13. (a) JOEL JSM-6490LA present at SCME; (b) SEM Schematic

It is most versatile and powerful technique for studying compounds in nano range. It can provide 3D image of topography and it can determine the height and thickness of nano compounds. It can produce images with the atomic resolution. It uses a tip attached to cantilever to scan a model surface. When tip comes near to sample surface, surface and tip deflects cantilever towards sample[30]. Tip makes contact with sample and repulsive forces arise which deflect the cantilever from the surface.

It uses a piezoelectric scanner for the scanning sample's surface. The feedback control system maintains a constant distance between tip and samples' surface. Optical –lever monitors defections from laser source on cantilever's back which is read by a sensitive photodiode. Vertical resolution is up to sub Å and lateral dimensions are up to 1nm.

The atomic force microscopy of prepared samples was done by **JOEL JSPM-5200** present at **SCME-NUST**. It was performed under tapping mode in air to have maximum tip-sample interaction. Micro-fabricated cantilevers were used **(NSC35; Mmasch)** with the respective values of the length, nominal tip radius, spring's constant, and the resonance frequency to 130 mm, 10 nm, 4.5 N/m, and 150 kHz. The materials to be analyzed were deposited on glass slide and they were dried under UV lamp. By this technique the length and height of samples were studied[31]. Also, morphology and particles uniformity on a fixed area can also be seen.

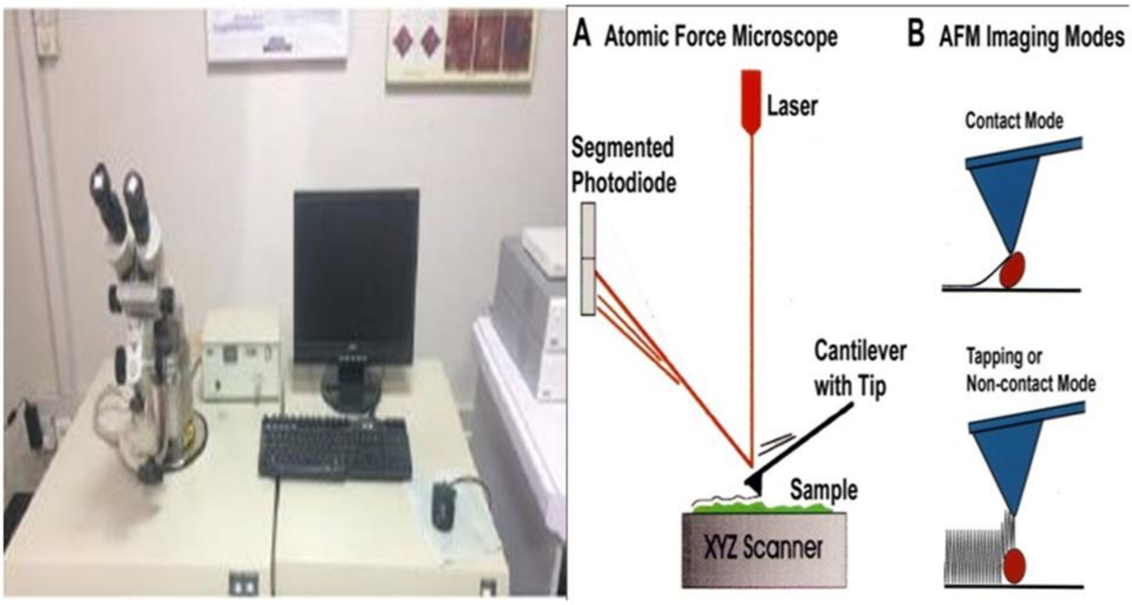

Figure:14. (a) Scanning Probe Microscope at SCME, NUST (b) AFM Schematics

3.3. X-ray diffraction (XRD)

It is critical technique which is used to determine the crystalline phase of the material. It is the non-destructive method and it provides fingerprints of Bragg's reflections of crystalline materials[32]. X-ray diffractometer consist of 3 basic elements. A cathode tube, sample holder and x-ray detector. X-rays are produced by heating filament element which accelerates electrons towards a target which collide with target material with electrons. Crystal is composed of layers and planes. So, x-ray which has wavelength having similar to these planes is reflected that angle of the incidence is equal to angle of reflection[33]. "Diffraction" takes place and it can be described as by Bragg's Law:

$2d\sin\theta = n\lambda$

When Bragg's law is fulfilled, the constructive interference takes place and "Bragg's reflections" will be picked up by the detector.These reflections positions tells about inter-layer spacing.X-ray diffraction tells us about the phase, crystallinity and sample purity. By this technique one can also determine lattice mismatch, dislocations and unit cell dimensions[34].

X-ray diffractions were performed by STOE diffractometer at SCME-NUST. The scan angle was 20^0 to 80^0

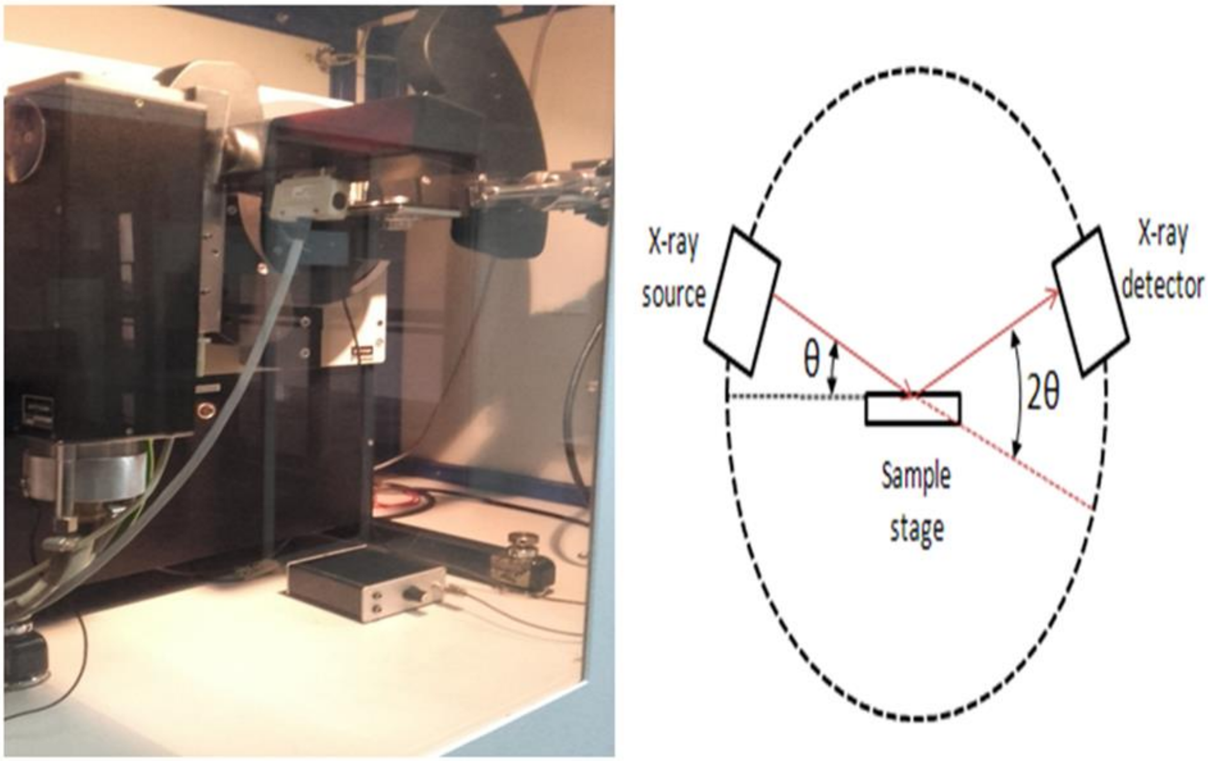

Figure:15. XRD present at SCME- NUST (b) XRD basic schematics

3.4. RAMAN Spectroscopy

Raman spectroscopy is the vibrational spectroscopy in which light interact with molecule to modify the polarizability of the molecule. Raman Result was first discovered by C.V. Raman and K.S. Krishnan in 1928. The technique is then grow to be a powerful tool to analyze chemical substances. When light of specific wavelength focus to the molecule the photons are scattered elastically and inelastically. Elastic scattering is termed as Rayleigh scattering. A portion of photons from incident beam (1 in 107 photons approx.) are scattered inelastically, called Raman affect, having lower energy (and frequency) than that of incident photons[35].Raman scattering happens by the alter in vibrational, rotational/electronic energy of molecule. The scattered photons are of lower energy than incident photons and the phenomenon is called Stokes shift. Since the small population is already in vibrational excited state, upon Raman scattering the molecule is then relaxed back to the ground state lower than the initial state, therefore the discharged photon has higher energy (smaller in wavelength) than incident photon[36]. This phenomenon is called Anti-Stokes shift. Anti-Stokes shift range is always lower than the Stokes shifted Raman spectrum at the room temperature, both have same frequency information, therefore Stokes shifted Raman spectrum is usually follows [37]. Fig-8 shows all these effect with electronic energy states.

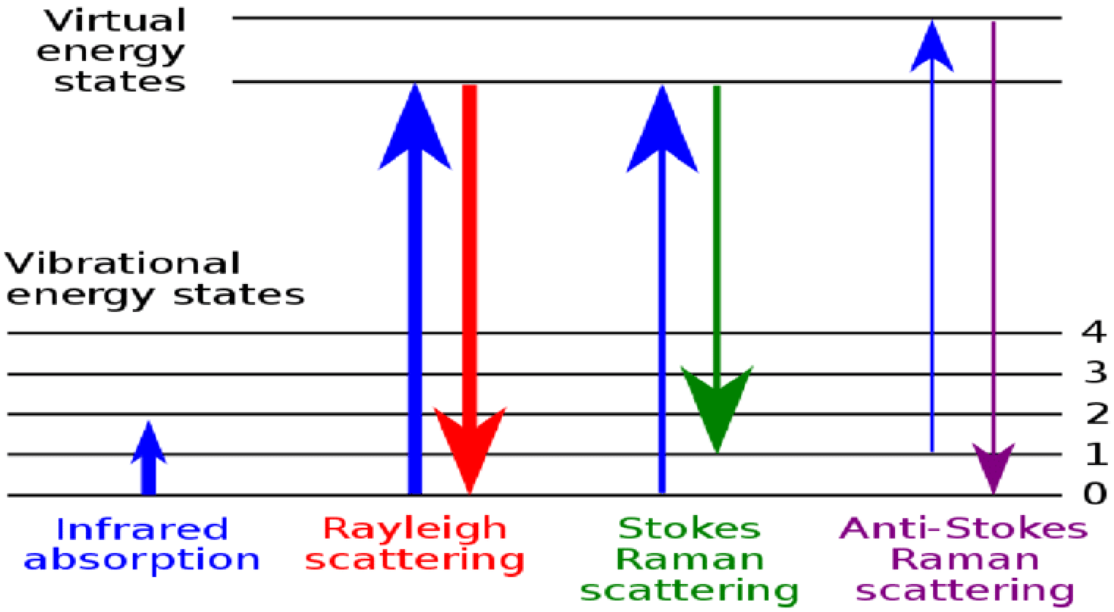

Figure:16.Energy level diagrams for Rayleigh scattering, Stokes Raman scattering and antiStokes Raman scattering

The main components of Raman spectrometer are a laser excitation source, excitation providingoptics, a sample, assortment optics, a wavelength partition device, a detector and related electronics and a recording tool. Raman spectrum is plot of the intensity of the Raman dispersed radiation as a function of its frequency variance from the incident radiation called Raman shift (units of wavenumbers, cm^{-1}).Raman spectroscopy is an important technique used to study Solids (units, pellets, powder, films, and fibers), liquid (gels, pastes) and gases in the area of biochemistry to material sciences[38].

Chapter 4

Results and Discussions

4.1. Schematic of Solar cell

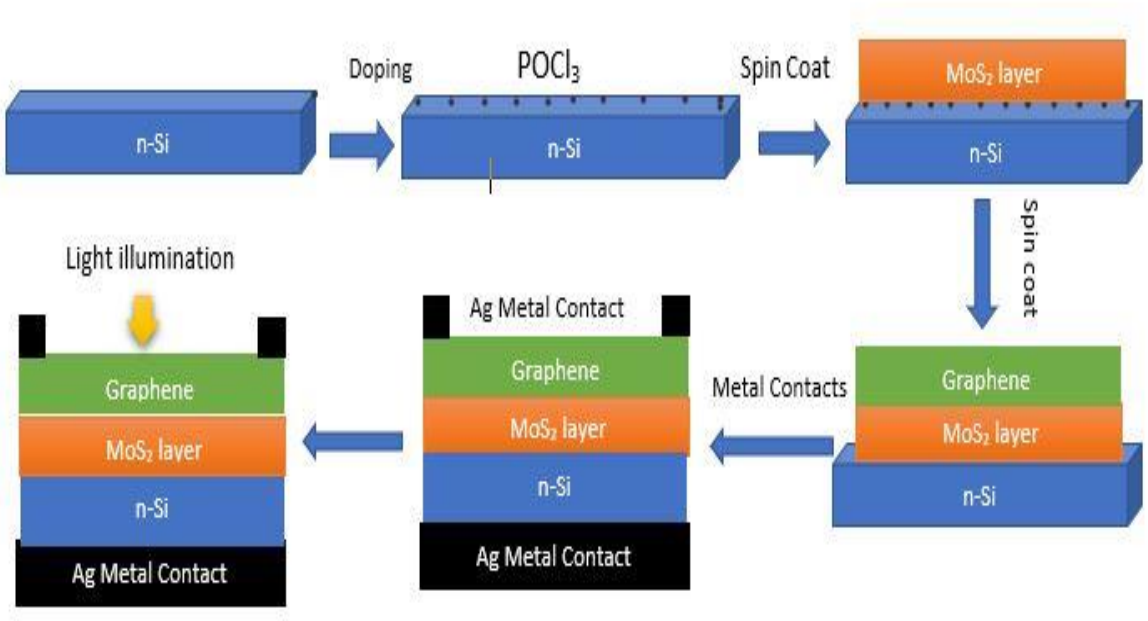

Figure: 17. Schematic of Device Fabrication

MoS_2 is exfoliated and Spin coat on Doped Silicon Substrate. After annealing Graphene is deposited by Spin coater. Silver Metal contacts is deposited by Sputtering Method. The cell is tested by under illumination of light.

4.2. XRDof MoS$_2$

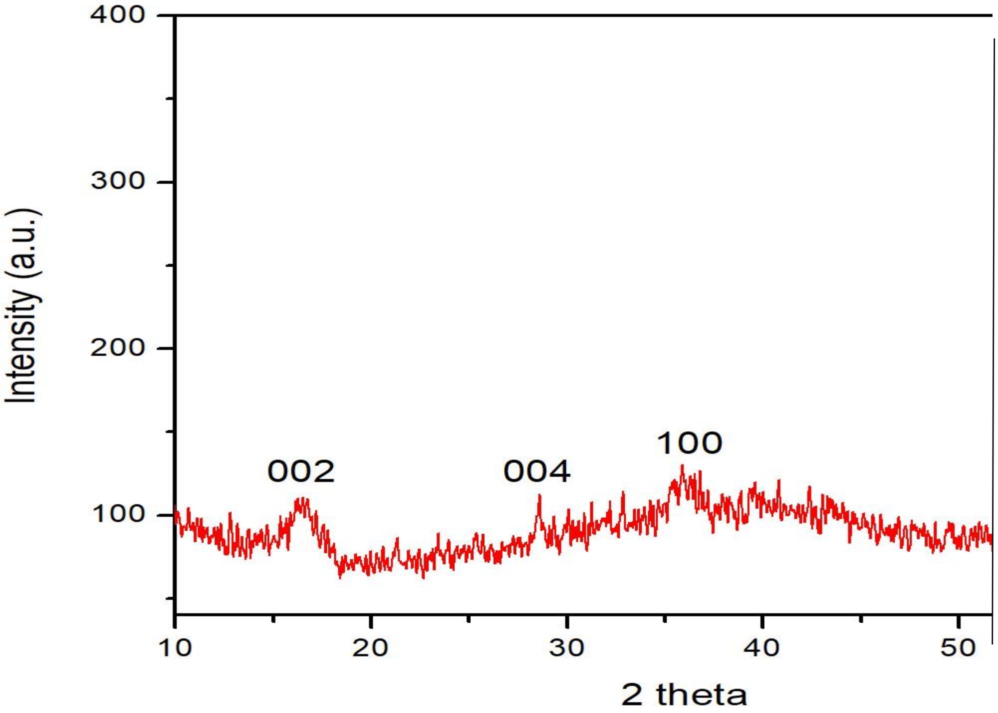

Figure: 18. XRD pattern of Exfoliated MoS$_2$

XRD was taken to study the structural and compositional evaluation of MoS$_2$. The peaks of XRD was matched with litraure and said succesfully synthesis of MoS2. There are four XRD modes appear in XRD spectrum of exfoliated MoS$_2$. These are the dominant modes of MoS$_2$. The [002] mode appear at 16^0 , [004] mode appear at 29^0 , [100] mode appear at 35^0.The peaks are not so intense this reflects the monolayer or bilayer presence of Exfoliated MoS$_2$.

4.3. Raman spectroscopy Of MoS_2:

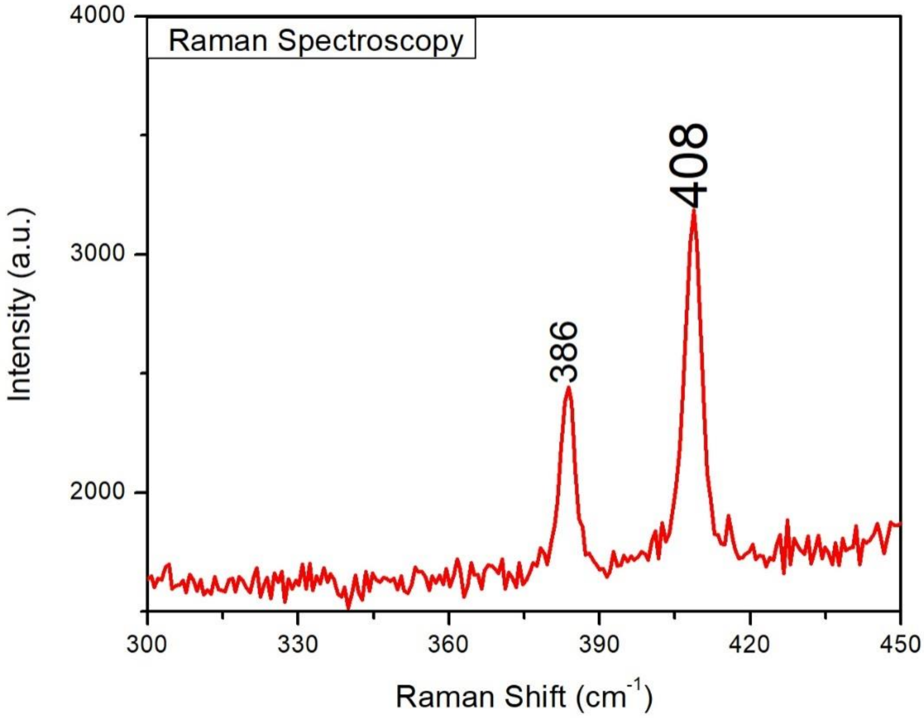

Figure: 19.Raman Spectroscopy of exfoliated MoS_2

MoS_2 holds 18 average Raman modes of vibration that found in literature, out of which only two strong modes found shown the strongest intensities. These two modes considered the feature modes of MoS_2. The In-plane E1 mode comes due to positive vibrations of one Mo atom and two S atoms, while the A1 mode comes due to out of plane vibration of the S atoms in reverse direction. The E1 and A1 is reliant on frequencies , the A1 Raman peak converts stiff with increasing number of the layers and E2 peak become soft with the increasing layers. The difference between the frequencies of two peaks used for identification of the layers number. The shift in Frequency connected to the thickness data of MoS_2 layers. For Exfoliated MoS_2 , the E1 and A1 peaks appeared at around 386 and 408 cm^{-1} respectively. The distinction between the frequencies of two peaks is 22 cm-1 which was an indication of multi-layer. The widen peak width of the modes also support the multilayer fact . Raman spectra reflects the MoS_2 presence.

4.4. AFM of MoS$_2$

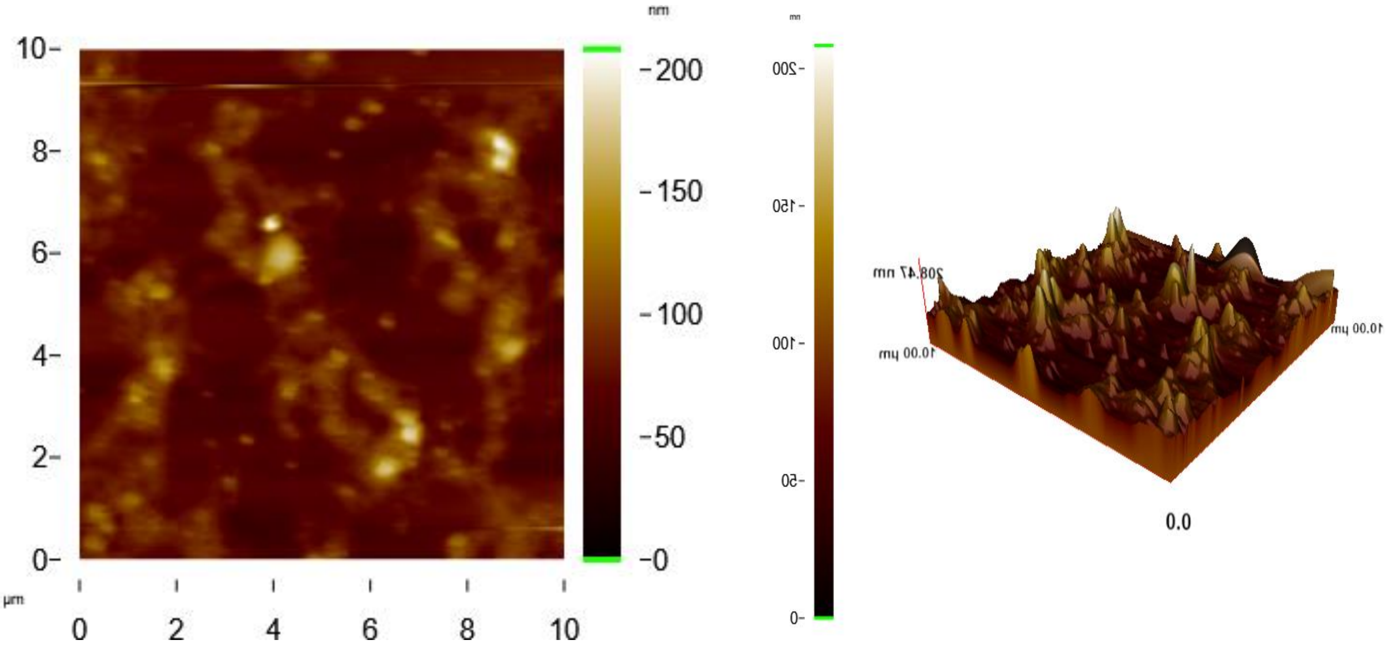

Figure: 20. Raman Spectroscopy of exfoliated MoS$_2$

AFM images of MoS2 shows the surface Morphology of Spin coat Film n Silicon substrate. The vertical scale is vary from 0 to 200 nm while the horizontal is 0 to 10 µm. Images shows the coated morphology on substrates and prepared device fabrication

4.5. SEM images of MoS_2

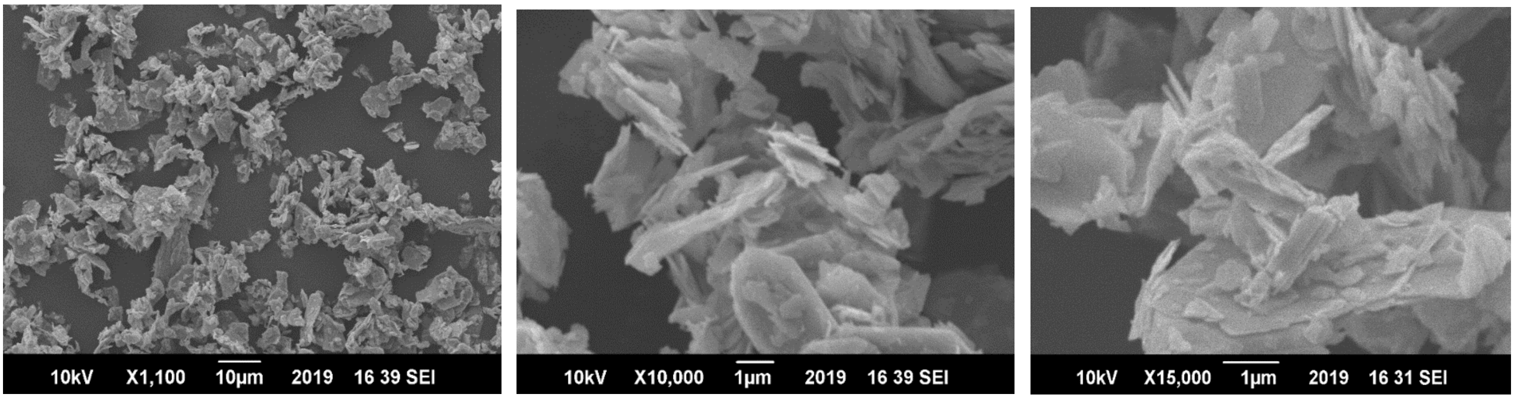

Figure:21. SEM images of MoS_2

The SEM images revealed the formation of nano structures. The low magnification images showed the uniformity found in materials. And high magnification image endorsed the formation of nanowires.

4.6. XRD of Graphene :

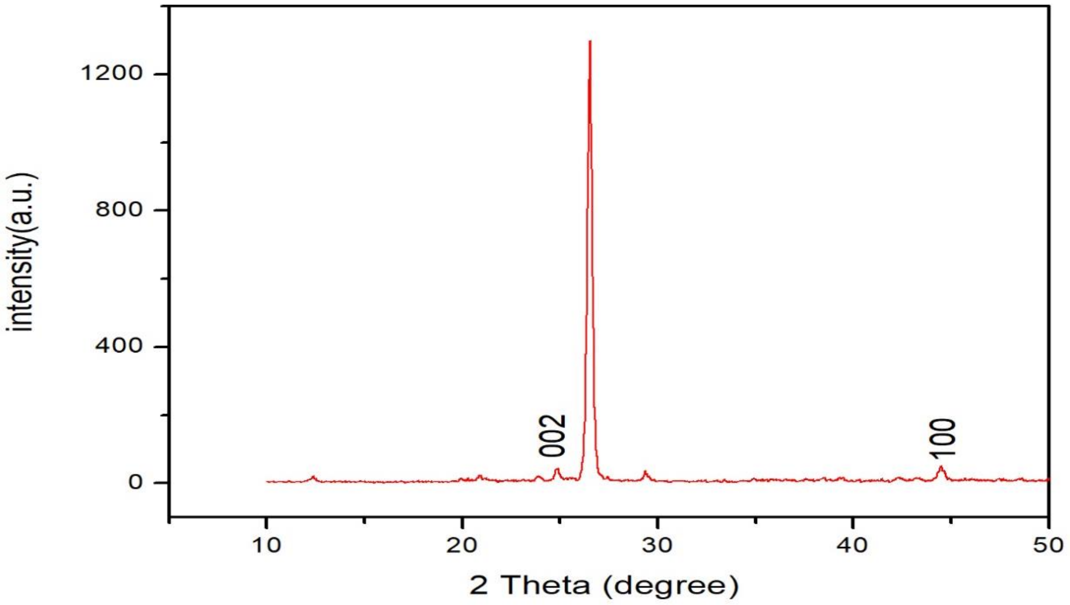

:Figure:22. XRD pattern of Graphene

The XRD of graphene was carried out to study the structure properties. There are two dominant modes present in XRD spectrum of graphene. The [002] plan appear around 35^0 and [100] plane appear around 44^0, these planes reflects the presence of graphene.

4.7. Raman of Graphene :

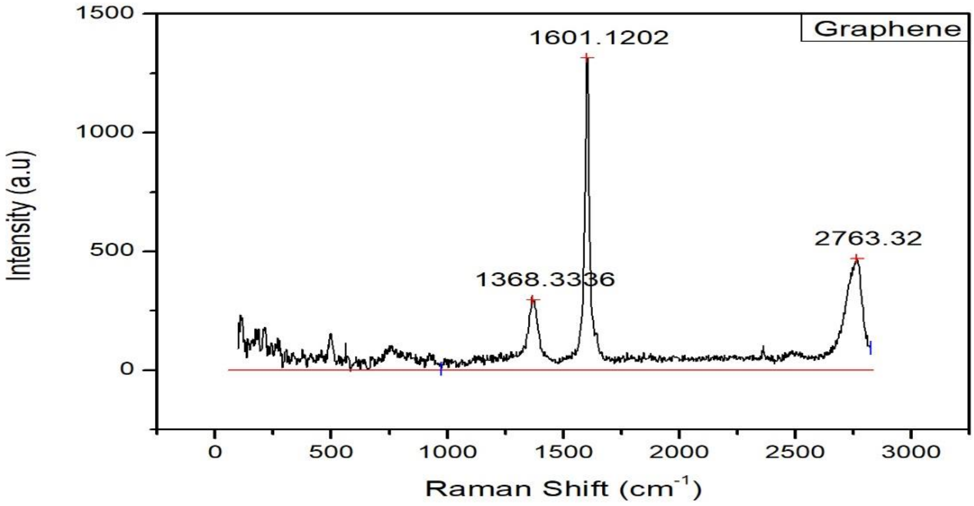

Figure:23. Raman Spectroscopy of Graphene

There are three modes are observed and these are considered as a featured modes of Graphene. As Graphene is produced by exfoliation of graphite, the peaks are not so intense because the graphene are single layer so it is very difficult to locate the intense peaks of graphene. , a mode at 1386 cm^{-1}, 1601 cm^{-1} and at 2763 cm^{-1} are the dominate modes of graphene and represent the presence of bilayer or multilayer of graphene.

4.8. SEMimages of Graphene:

4.8.1. By Exfoliation Method:

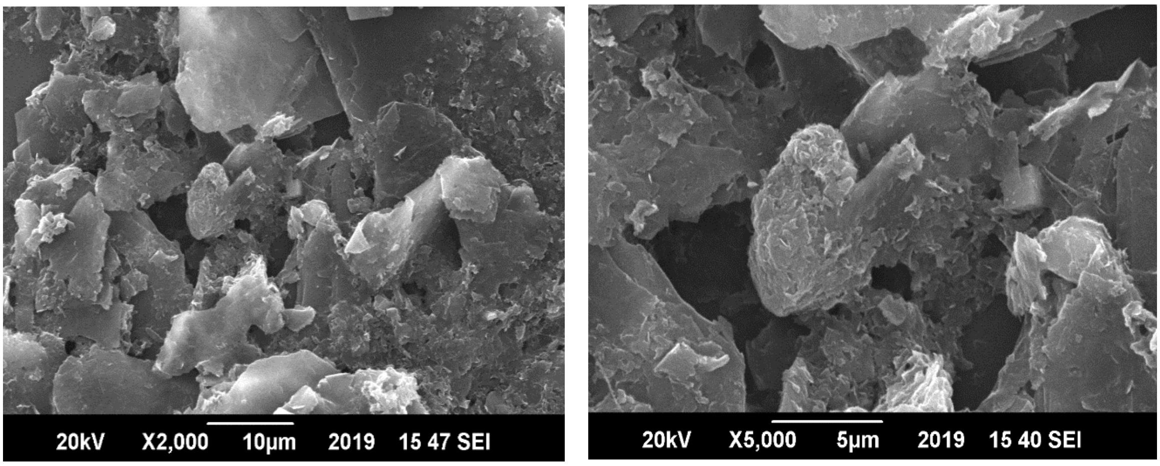

Figure: 24. SEM images of Graphene

SEM analysis waredoneutilizing scanning electron microscope (JEOL- JSM- 6490LA) with operating voltage of 10-20 kV. There are graphene flakes clearly seen. The images were detailed in SE mode at low and the high magnifications. In low resolution image flakes seen ebbed one another and these flakes are dominant.

4.9. Solar Cell :

4.9.1 I-V curve results.

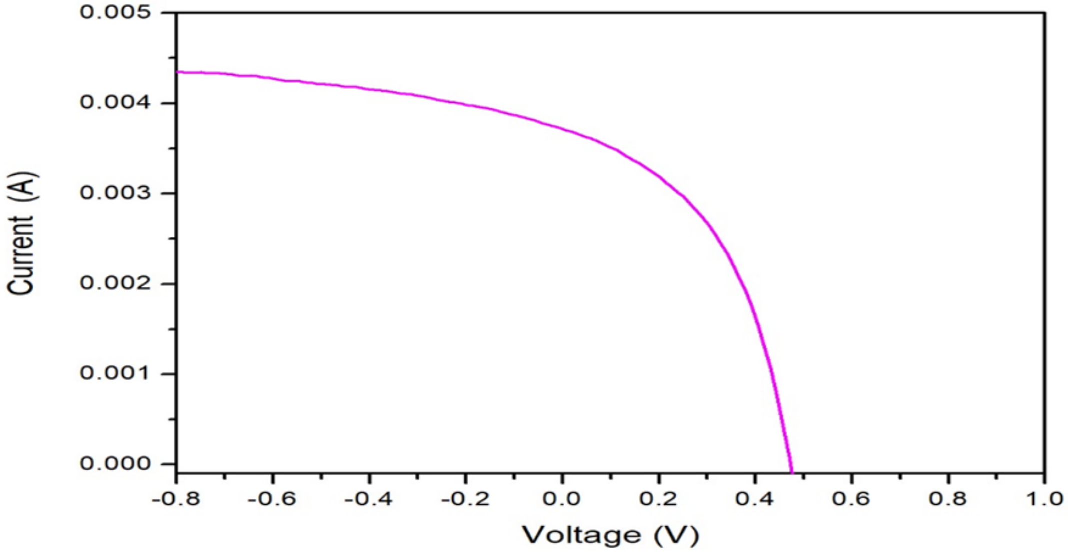

Figure: 25. I-V curve for solar cell shows 4.02 efficiency

I-V curve reflects the photovoltaic performance of cell under light. This calculated efficiency for this curve is η = 4.020691%. The open circuit voltage V_{oc} is 0.47 V and I_{sc} is 3.7mA . Fill factor is around 45.5% and short circuit current density J_{sc} (mA/cm2) is 18.606. which leads the photovoltaic performance of cell. The maximum power P_{max} is 0.81 mW generated. This represents the electron hole pair generated as a result of light falls on the surface of cell.

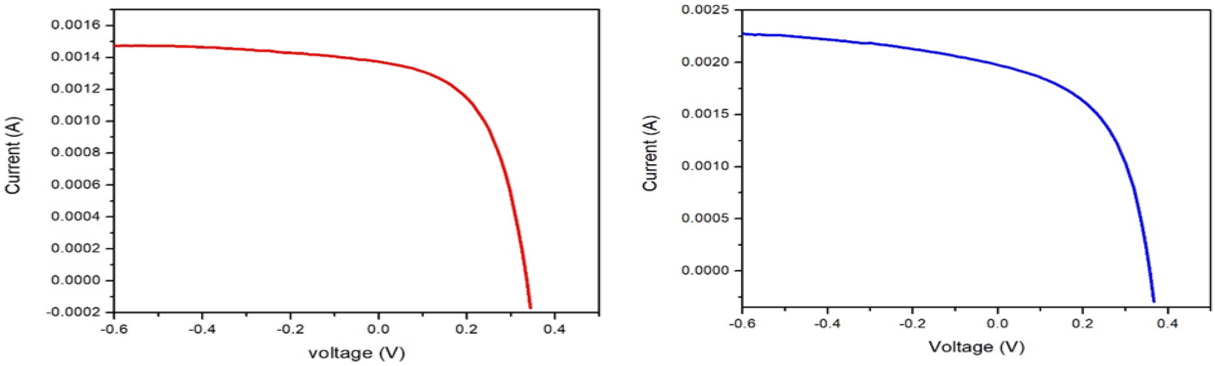

Figure: 26. (a)I-V curve of solar cell reflects efficiency around 0.22% (b) I-V curve of solar cell reflects efficiency around 3.54%

In fig-24 (a) the IV curve shoes the photovoltaic performance cell under light. The calculated efficiency for this curve is η = 0.22%. The open circuit voltage Voc is 0.356 V and Isc is 1.3 mA . As the efficiency is low but the fill factor is quite well that is 56.27%.the short circuit current density Jsc (mA/cm2) is 1.12. while in fig-24 (b) the iv curve under light shows the calculated efficiency η = 3.54 % that is quite high as compared to monolayer spin coat sample The open circuit voltage Voc is 0.35 V and Isc is 1.9 mA .the Fill Factor is 50.12%.The short circuit current density Jsc (mA/cm2) is 19.789. The multilayer coating of graphene effects the parameters of photovoltaic cell.

References

[1] N. Gupta, G. Alapatt, R. Podila, R. Singh, and K. J. I. J. o. P. Poole, "Prospects of nanostructure-based solar cells for manufacturing future generations of photovoltaic modules," vol. 2009, 2009.

[2] T. Feng *et al.*, "Graphene based Schottky junction solar cells on patterned silicon-pillar-array substrate," vol. 99, no. 23, p. 233505, 2011.

[3] S. Glunz, S. Janz, M. Hofmann, T. Roth, and G. Willeke, "Surface passivation of silicon solar cells using amorphous silicon carbide layers," in *2006 IEEE 4th World Conference on Photovoltaic Energy Conference*, 2006, vol. 1, pp. 1016-1019: IEEE.

[4] J.-Y. Lin, C.-Y. Chan, and S.-W. J. C. c. Chou, "Electrophoretic deposition of transparent MoS 2–graphene nanosheet composite films as counter electrodes in dye-sensitized solar cells," vol. 49, no. 14, pp. 1440-1442, 2013.

[5] M. Mahjouri-Samani *et al.*, "Pulsed laser deposition of photoresponsive two-dimensional GaSe nanosheet networks," vol. 24, no. 40, pp. 6365-6371, 2014.

[6] P. P. J. T. f. p. I. Chow, "Molecular beam epitaxy," pp. 133-176, 1991.

[7] J. Kong, A. M. Cassell, and H. J. C. P. L. Dai, "Chemical vapor deposition of methane for single-walled carbon nanotubes," vol. 292, no. 4-6, pp. 567-574, 1998.

[8] X. Dong *et al.*, "Growth of large-sized graphene thin-films by liquid precursor-based chemical vapor deposition under atmospheric pressure," vol. 49, no. 11, pp. 3672-3678, 2011.

[9] K. Reichelt and X. J. T. S. F. Jiang, "The preparation of thin films by physical vapour deposition methods," vol. 191, no. 1, pp. 91-126, 1990.

[10] C. Liu, A. Leyland, Q. Bi, A. J. S. Matthews, and C. Technology, "Corrosion resistance of multi-layered plasma-assisted physical vapour deposition TiN and CrN coatings," vol. 141, no. 2-3, pp. 164-173, 2001.

[11] E. Andrade and M. J. T. S. F. Miki-Yoshida, "Growth, structure and optical characterization of high quality ZnO thin films obtained by spray pyrolysis," vol. 350, no. 1-2, pp. 192-202, 1999.

[12] C. Naşcu, I. Pop, V. Ionescu, E. Indrea, and I. J. M. l. Bratu, "Spray pyrolysis deposition of CuS thin films," vol. 32, no. 2-3, pp. 73-77, 1997.

[13] P. Xiao, M. Xiao, and K. J. P. Gong, "Preparation of exfoliated graphite/polystyrene composite by polymerization-filling technique," vol. 42, no. 11, pp. 4813-4816, 2001.

[14] W. Feng, P. Long, Y. Feng, and Y. J. A. S. Li, "Two-dimensional fluorinated graphene: synthesis, structures, properties and applications," vol. 3, no. 7, p. 1500413, 2016.

[15] A. Ciesielski and P. J. C. S. R. Samorì, "Graphene via sonication assisted liquid-phase exfoliation," vol. 43, no. 1, pp. 381-398, 2014.

[16] J. N. J. A. F. M. Coleman, "Liquid-phase exfoliation of nanotubes and graphene," vol. 19, no. 23, pp. 3680-3695, 2009.

[17] A. B. Bourlinos, V. Georgakilas, R. Zboril, T. A. Steriotis, and A. K. J. s. Stubos, "Liquid-phase exfoliation of graphite towards solubilized graphenes," vol. 5, no. 16, pp. 1841-1845, 2009.

[18] S. Eigler *et al.*, "Wet chemical synthesis of graphene," vol. 25, no. 26, pp. 3583-3587, 2013.

[19] Y. Zhang, K. Fugane, T. Mori, L. Niu, and J. J. J. o. M. C. Ye, "Wet chemical synthesis of nitrogen-doped graphene towards oxygen reduction electrocatalysts without high-temperature pyrolysis," vol. 22, no. 14, pp. 6575-6580, 2012.

[20] L. C. Klein, *Sol-gel optics: processing and applications*. Springer Science & Business Media, 2013.

[21] D.-H. Chen and X.-R. J. M. R. B. He, "Synthesis of nickel ferrite nanoparticles by sol-gel method," vol. 36, no. 7-8, pp. 1369-1377, 2001.

[22] A. Jawaid *et al.*, "Mechanism for liquid phase exfoliation of MoS2," vol. 28, no. 1, pp. 337-348, 2016.

[23] A. Gupta, V. Arunachalam, and S. J. T. j. o. p. c. l. Vasudevan, "Liquid-phase exfoliation of MoS2 nanosheets: The critical role of trace water," vol. 7, no. 23, pp. 4884-4890, 2016.

[24] S.-L. Zhang, H. Jung, J.-S. Huh, J.-B. Yu, W.-C. J. J. o. n. Yang, and nanotechnology, "Efficient exfoliation of MoS2 with volatile solvents and their application for humidity sensor," vol. 14, no. 11, pp. 8518-8522, 2014.

[25] X. Fan *et al.*, "Controlled exfoliation of MoS2 crystals into trilayer nanosheets," vol. 138, no. 15, pp. 5143-5149, 2016.

[26] C. C. Mayorga-Martinez, A. Ambrosi, A. Y. S. Eng, Z. Sofer, and M. J. E. C. Pumera, "Transition metal dichalcogenides (MoS2, MoSe2, WS2 and WSe2) exfoliation technique has strong influence upon their capacitance," vol. 56, pp. 24-28, 2015.

[27] X. Feng *et al.*, "Liquid-exfoliated MoS2 by chitosan and enhanced mechanical and thermal properties of chitosan/MoS2 composites," vol. 93, pp. 76-82, 2014.

[28] K. Takahashi, K. Yamada, H. Kato, H. Hibino, and Y. J. S. s. Homma, "In situ scanning electron microscopy of graphene growth on polycrystalline Ni substrate," vol. 606, no. 7-8, pp. 728-732, 2012.

[29] Z. Wu *et al.*, "Enhanced sensitivity of ammonia sensor using graphene/polyaniline nanocomposite," vol. 178, pp. 485-493, 2013.

[30] M. Krueger *et al.*, "Drop-casted self-assembling graphene oxide membranes for scanning electron microscopy on wet and dense gaseous samples," vol. 5, no. 12, pp. 10047-10054, 2011.

[31] P. Nemes-Incze, Z. Osváth, K. Kamarás, and L. J. C. Biró, "Anomalies in thickness measurements of graphene and few layer graphite crystals by tapping mode atomic force microscopy," vol. 46, no. 11, pp. 1435-1442, 2008.

[32] G. Huang *et al.*, "Graphene-Like MoS2/Graphene Composites: Cationic Surfactant-Assisted Hydrothermal Synthesis and Electrochemical Reversible Storage of Lithium," vol. 9, no. 21, pp. 3693-3703, 2013.

[33] L. David, R. Bhandavat, and G. J. A. n. Singh, "MoS2/graphene composite paper for sodium-ion battery electrodes," vol. 8, no. 2, pp. 1759-1770, 2014.

[34] B. E. Warren, *X-ray Diffraction*. Courier Corporation, 1990.

[35] A. C. Ferrari *et al.*, "Raman spectrum of graphene and graphene layers," vol. 97, no. 18, p. 187401, 2006.

[36] H. Li *et al.*, "From bulk to monolayer MoS2: evolution of Raman scattering," vol. 22, no. 7, pp. 1385-1390, 2012.

[37] X. Ling *et al.*, "Raman enhancement effect on two-dimensional layered materials: graphene, h-BN and MoS2," vol. 14, no. 6, pp. 3033-3040, 2014.

[38] Y. Wang, C. Cong, C. Qiu, and T. J. s. Yu, "Raman spectroscopy study of lattice vibration and crystallographic orientation of monolayer MoS2 under uniaxial strain," vol. 9, no. 17, pp. 2857-2861, 2013.